Drug Design, Development and Therapy

Dovepress
Taylor & Francis Group

Open Access Full Text Article

ORIGINAL RESEARCH

Modified Zuo Gui Wan Ameliorates Ovariectomy-Induced Osteoporosis in Rats by Regulating the SCFA-GPR41-p38MAPK Signaling Pathway

Changheng Song[1,2,*], Qiqi Yan[1,*], Yujie Ma[3], Pei Li[1], Ying Yang[1], Yuhan Wang[1], Wenjie Li[1], Xinyu Wan[1], Yubo Li[1], Ruyuan Zhu[1], Haixia Liu[1], Zhiguo Zhang[1]

[1]Institute of Basic Theory for Chinese Medicine, China Academy of Chinese Medical Sciences, Beijing, People's Republic of China; [2]Department of Endocrinology, Guang'anmen Hospital, China Academy of Chinese Medical Sciences, Beijing, People's Republic of China; [3]Science and Technology Innovation Center, Guangzhou University of Chinese Medicine, Guangzhou, People's Republic of China

*These authors contributed equally to this work

Correspondence: Haixia Liu; Zhiguo Zhang, Institute of Basic Theory for Chinese Medicine, China Academy of Chinese Medical Sciences, No. 16, DongzhimenNei Nanxiaojie Street, Dongcheng District, Beijing, 100700, People's Republic of China, Email lhx8866_7@163.com; zzgtcm@163.com

Objective: Modified Zuo Gui Wan (MZGW) was a combination of Zuo Gui Wan and red yeast rice used for treating osteoporosis (OP), but its mechanism remains unclear. We aimed to validate the anti-OP effect of MZGW and explore its underlying mechanism.

Methods: An ovariectomy (OVX) rat model in vivo and a RANKL-induced osteoclasts (OCs) model in vitro were established. Key active ingredients in MZGW high dose (MZGW-H) group were detected by UPLC-MS/MS. Micro-CT scans and histomorphology analysis were performed in OVX rats. 16S rRNA gene sequencing was performed to investigate the relationship between the anti-OP effect of MZGW-H and intestinal flora. CCK-8 assay was applied to examine the optimal concentration of Modified Zuo Gui Wan drug serum (MZGW-DS) on osteoclasts. The qRT-PCR and Western blotting were utilized to explore the potential anti-OP pathway of MZGW, namely the SCFA-GPR41-p38MAPK signaling pathway. GPR41 was knocked down to further reverse to verify whether the pathway was the key pathway for MZGW-DS to exert its inhibitory effect on osteoclasts.

Results: The three main blood components, Ferulic acid, L-Ascorbic acid and Riboflavin, were examined mainly by UPLC-MS/MS. 16S rRNA gene sequencing showed that MZGW-H changed the metabolism of SCFAs. In vivo studies verified that MZGW-H ameliorated microstructure damage, improved histological changes and reduced TRAP, BALP, and BGP in OVX rats by regulating the SCFA-GPR41-p38MAPK signaling pathway. CCK-8 revealed that 5% MZGW-DS group was the most optimal concentration of MZGW-DS to inhibit osteoclast differentiation. In vitro, MZGW-DS was better than peripheral blood concentration of SCFAs in inhibiting osteoclasts. After the knockout of GPR41, MZGW-DS could not inhibit the expression of osteoclast-related protein (CTSK and NFATc1) via SCFA-GPR41-p38MAPK signaling pathway.

Conclusion: MZGW-H effectively ameliorates OVX-induced osteoporosis partially achieved by increasing SCFAs metabolism and modulating the SCFA-GPR41-p38MAPK signaling pathway.

Keywords: osteoporosis, short chain fatty acids, SCFA-GPR41-p38MAPK signaling pathway, osteoclasts, modified Zuo Gui Wan

Introduction

Osteoporosis (OP) is a bone metabolism disorder accompanied by a high incidence and a serious fracture risk, posing a severe threat to the health and quality of life of postmenopausal women.[1] With the rapid increase in the aging population worldwide, OP has emerged as a global public health issue.[2] Preliminary research conducted by our group has revealed that ovariectomy (OVX)-induced OP rats present metabolic disorders such as intestinal microbial metabolism, in addition to bone metabolism,[3] just as confirmed in the other research.[4] Moreover, OP is aggravated by changes in the

Received: 26 September 2024
Accepted: 14 December 2024
Published: 27 December 2024

© 2024 Song et al. This work is published and licensed by Dove Medical Press Limited. The full terms of this license are available at https://www.dovepress.com/terms.php and incorporate the Creative Commons Attribution – Non Commercial (unported, v3.0) License (http://creativecommons.org/licenses/by-nc/3.0/). By accessing the work you hereby accept the Terms. Non-commercial uses of the work are permitted without any further permission from Dove Medical Press Limited, provided the work is properly attributed. For permission for commercial use of this work, please see paragraphs 4.2 and 5 of our Terms (https://www.dovepress.com/terms.php).

Graphical Abstract

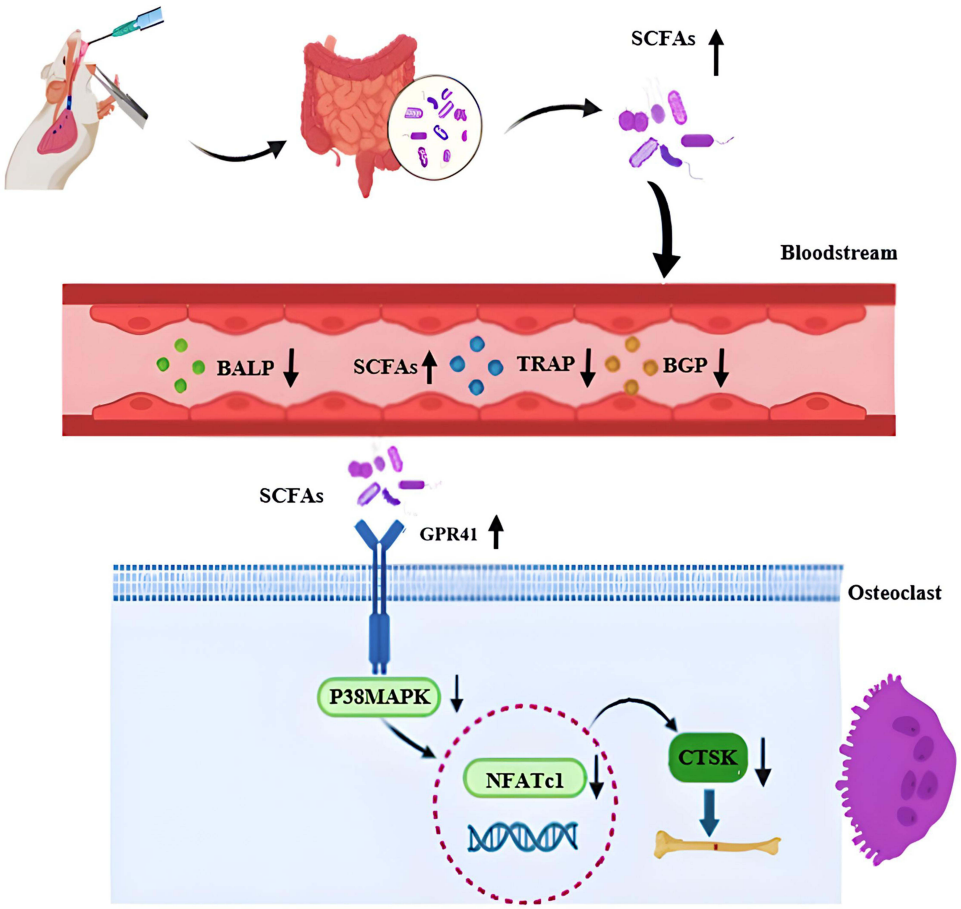

diversity and dysfunction of intestinal flora. Considering the potency and side effects of existing drugs, developing new anti-OP drugs is necessary.

Zuo Gui Wan is a renowned "kidney tonic" formula in Chinese medicine, and an increasing number of clinical and animal experimental studies have substantiated its anti-OP effect.[5–7] Additionally, modern studies have found that red yeast rice can ameliorate intestinal flora dysbiosis,[8–10] promote bone formation, and increase bone mineral density.[11] Hence, considering these findings, we incorporated red yeast rice into the original Zuo Gui Wan formula, resulting in the modified Zuo Gui Wan (MZGW). The preliminary research has validated the anti-OP effect of MZGW, but the mechanism remains incompletely understood.

With the concept of the "intestinal-bone" axis, the correlation among intestinal flora, short-chain fatty acids (SCFAs), and bone metabolism has been established.[12] OP is accompanied by changes in intestinal flora, and dysfunctions in intestinal flora can aggravate or induce OP.[13,14] Additionally, SCFAs serve as biomarkers of bone metabolic activity, and supplementation with probiotics or prebiotics can alter intestinal flora composition to modulate SCFAs and improve bone mass.[15,16] SCFAs regulate osteoclast (OC) metabolism and bone mass in vivo, inhibit OC differentiation and bone resorption, whereas bone formation is unaffected.[17] GPR41, a Gi/o protein-coupled receptor, is a key receptor for SCFAs binding and regulates inflammatory responses.[18,19] Butyric acid (an SCFA) binds to the GPR41 receptor, inhibiting osteoclastogenesis and alleviating osteolysis.[20] Moreover, SCFAs attenuate the inflammatory response by reducing the phosphorylation of p38 and JNK in a GPR41/43-dependent manner, thereby preventing renal inflammation.[21] Signaling mediated by mitogen-activated protein kinases (MAPK), including extracellular signal-regulated kinase (ERK), c-Jun

N-terminal kinase (JNK), and p38, has been suggested to be critical for normal OC differentiation and activation.[22] However, whether SCFAs can reduce p38 phosphorylation and inhibit osteoclastogenesis in a GPR41-dependent manner remains unknown. In our study, we hypothesized that the SCFAs in MZGW may bind to the specific receptor GPR41 on the surface of OCs, inhibiting the p38MAPK-NFATc1 OC differentiation pathway, ultimately impeding osteoclastogenesis and exerting anti-OP effects.

Materials and Methods

Preparation of MZGW

The composition of MZGW was as follows: Rehmanniae Radix Praeparata (24 g), Dioscoreae Rhizoma (12 g), Lycium barbarum (12 g), Corni Fructus (12 g), Cervi Cornus Colla (12 g), Testudinis Carapaxet Plastic Collar (12 g), Cuscuta chinensis (12 g), Achyranthes bidentata (9 g), and Monascus purpureus Went (15 g) (Table 1). Cervi Cornus colla and Testudinis carapaxet plastic collar were cured, and the remaining herbs were decocted in pure water and concentrated to obtain a concentration of 1.08 g crude herbs/mL MZGW. All these components of traditional Chinese medicine were purchased from Beijing Tongrentang Medicinal Materials Co., Ltd. (Beijing, China).

Ultra Performance Liquid Chromatography–Tandem Mass Spectrometry

The high concentration of MZGW extract (1.08 g crude herbs/mL) was analyzed using ultra performance liquid chromatography–tandem mass spectrometry (UPLC-MS/MS). The analysis utilized an Agilent SB-C18 UPLC column (1.8 μm, 2.1 mm * 100 mm). The mobile phase comprised solvent A, consisting of pure water with 0.1% formic acid, and solvent B, consisting of acetonitrile with 0.1% formic acid. Sample measurements were performed with a gradient program starting at 95% A and 5% B. Within 9 min, a linear gradient to 5% A and 95% B was programmed, and a composition of 5% A and 95% B was maintained for 1 min. Subsequently, a composition of 95% A and 5% B was adjusted within 1.1 min and maintained for 2.9 min. The flow velocity was set at 0.35 mL per minute; the column oven was set to 40°C; and the injection volume was 2 μL. The effluent was alternatively connected to an ESI-triple quadrupole-linear ion trap (QTRAP)-MS.

OVX Animal Model

The treatment of all animals in this experiment was approved by the Institutional Ethics Committee of the China Academy of Chinese Medical Sciences (ethics approval number: IBTCMCACMS21-2104-03). Sixty female Sprague–Dawley rats, aged 3 months and weighing 180–220 g, were provided by Beijing Vital River Laboratory Animal Technology Co., Ltd. (SCXK (Jing) 2019–0009, Beijing, China). The rats were kept at a relative temperature of 20°C–25°C and relative humidity of 45%–60%, with a 12 h:12 h intermittent lighting day and night. They had free access to food and water. After 1 week of environmental acclimatization, rats were randomly divided into 6 groups (n=10) according to body weight: the negative control group (NC, distilled water, 1 mL/100 g), sham-operation group (SHAM, sham-operated rats+distilled water, 1 mL/100 g), model group (OVX, OVX rats+distilled water, 1 mL/100 g),

Table 1 Composition of MZGW

Chinese Name	Latin Name	Weight(g)
Shu Di Huang	Rehmanniae Radix Praeparata	24
Shan Yao	Dioscoreae Rhizoma	12
Gou Qi	Lycium barbarum	12
Shan Yu Rou	Corni Fructus	12
Lu Jiao	Cervi Cornus Colla	12
Gui Ban Jiao	Testudinis Carapaxet Plastic Collar	12
Tu Si Zi	Cuscuta chinensis	12
Niu Xi	Achyranthes bidentata	9
Hong Qu	Monascus purpureus Went	15

estradiol valerate group (EV, OVX rats+estradiol valerate, 0.18 mg/kg; Bayer Healthcare, Guangzhou, China), MZGW low-dose (MZGW-L) group (MZGW-L, OVX rats+MZGW-L, 5.4 g/kg) and MZGW high-dose (MZGW-H) group (MZGW-H, OVX rats+MZGW-H, 10.8 g/kg). Rats were treated with once daily gavage for 3 months.

Sample Collection and Storage

During the last three days of the experiment, fresh feces of rats (4–5 pieces per rat) were continuously collected and frozen at −80°C until 16S ribosomal RNA (rRNA) gene sequencing was performed. After drug administration, rats were anesthetized by intraperitoneal injection of pentobarbital sodium (3%, 0.14 mL/100 g). Arterial blood was collected, and serum was centrifuged at 3000 rpm for 10 min at 4°C and stored at −80°C until further analysis. Femurs were removed and soaked in 4% paraformaldehyde for hematoxylin-eosin (HE) staining, tartrate-resistant acid phosphatase (TRAP) staining, and micro-computed tomography (micro-CT) analyses. Tibias were removed and preserved at −80°C for quantitative reverse transcription PCR (qRT-PCR) and Western blotting (WB).

Preparation of the Serum Containing MZGW

After 7 days of adaptive feeding, 40 female SD rats, aged 3 months and weighing 180–220 g, were randomly divided into two groups according to body weight: 10 rats in the NC group and 30 rats in the modeling group. Rats in the modeling group underwent debridement surgery (bilateral OVX). One week after surgery, rats in the modeling group were divided into the OVX group (15 rats) and MZGW-H group (15 rats), with administration by gavage as previously described in 2.3. One hour after the last administration, the rats were anesthetized using pentobarbital sodium intraperitoneally. Rat blood samples were collected from the abdominal aorta and centrifuged at 3,000 rpm/min at 4°C for 20 min. Serum was collected and filtered through a 0.22 um filter, heat-inactivated at 56°C for 30 min, and stored at −80°C until use.

Bone Micro-Architecture Assessment Through Micro-CT

The right femurs were scanned using a micro-CT scanner (SkyScan1276, Bruker, USA) and evaluated using the analysis software. Bone parameters, including bone mineral density (BMD, g/cm^3), relative bone volume (BV/TV, %), trabecular number (Tb.N, 1/mm), and trabecular separation (Tb.Sp, mm), were calculated for rats, using the software.

Histomorphology Analysis

HE Staining

The left femur was fixed in 4% paraformaldehyde (Biosharp, China) and decalcified in 10% EDTA (Biosharp). The femur was embedded in paraffin and sliced with a thickness of 5 μm. Sections were then dewaxed, stained, and viewed under a microscope (Leica, German).

TRAP Staining

The paraffin sections of decalcified bone were dewaxed to water, immersed in TRAP staining solution (Solarbio, Beijing) for 3 h at 37°C, and restained with hematoxylin. The sections were dehydrated, made transparent, and sealed. Five visual fields were randomly selected under an inverted microscope to observe the distribution, morphology, and number of $TRAP^+OCs$.

Toluidine Blue Staining

RAW264.7 cells were inoculated on the prepared bovine bone slices and induced into osteoclasts, and then serum and SCFAs from each group of rats was added. All slices were sonicated with 0.25 mol/L ammonia solution, and washed with PBS on the seventh day, dried, and then incubated at room temperature for 10 min by adding 1% toluidine blue staining solution (Solarbio, China), and rinsed clean with pure water. The number and morphology of the area of bone resorption lacunae were observed under the microscope, and the area of bone resorption lacunae was calculated.

Detection of Serum Indicators

Serum levels of TRAP (FANKEWEI, China), bone alkaline phosphatase (BALP; FANKEWEI), and bone gamma-carboxyglutamic acid-containing protein (BGP; FANKEWEI) were determined using enzyme-linked immunoassay (ELISA) kits, following the manufacturer's instructions.

qRT-PCR Analysis

The expression of key factors of the p38 pathway in OVX rats and OCs was determined. Total RNA was extracted from the tibia, using Trizol Reagent (Takara, Japan). The extracted RNA was reverse transcribed into cDNA using an oligo (dT) primer and M-MLV Reverse Transcriptase (Takara). The qPCR reaction was performed using the qPCR SYBR Green Master Mix kit (YEASEN, China), according to the manufacturer's instructions. The relative expression levels of mRNA were calculated using the $2^{-\Delta\Delta Ct}$ method. The primer sequences of each gene are provided in Table 2.

WB Analysis

WB was used to detect the expression of key factors of the GPR41 and p38 pathways in OVX rats and OCs. The samples were lysed with RIPA agents (APPLYGEN, China), and protein concentrations were determined using the QuantiPro BCA assay kit (YEASEN). After electrophoresis with 8% SDS-PAGE (APPLYGEN), proteins were transferred to a PVDF membrane and blocked with 5% skimmed milk/BSA (APPLYGEN) for 1 h. Subsequently, proteins were incubated with primary antibodies against β-actin (1:10,000, Proteintech, China), GPR41 (1:500, Proteintech), p38 (1:1000, Proteintech), p-p38 (1:1000, Proteintech), CTSK (1:1000, Proteintech), and NFATc1 (1:1000, Proteintech) at 4°C overnight, followed by washing three times rapidly with TBST. The membrane was then incubated with the corresponding horseradish peroxidase-conjugated secondary antibody (1:5000, Proteintech) for 1 h. ECL emitting solution (APPLYGEN) was prepared, and blotting results were captured using a BIO-RAD gel imaging system. Image analysis was performed using Image Lab software.

Analysis of the Diversity of Intestinal Flora

Deoxyribonucleic acid (DNA) extraction and library construction were performed using 16S rRNA gene sequencing. Genomic DNA served as a template to amplify the 16S V3-V4 region using Tks Gflex DNA polymerase (upstream primer: 5′-TACGGRAGGCAGCAG-3′, downstream primer: 5′-AGGGGTATCTAATCCT-3′, length: 455 bp). The PCR products were quantified using Qubit, aliquoted according to PCR product concentration, sequenced, OTU clustered, and annotated. They were then subjected to alpha and beta diversity analyses and other statistical analyses to identify differences between the samples.

Cell Culture and Grouping

For the induction of OCs, 50 ng/mL of RANKL (R&D, USA) was used. RAW264.7 cells were cultured in α-MEM (Gibco, USA) culture containing 10% FBS (Gibco) and inoculated in 24-well plates at a density of 2×10^4cells/well. After 24 h, the complete medium containing 50 ng/mL RANKL was added for induction. The rat serum groups comprised the negative normal serum (NC-S), ovariectomy serum (OVX-S), and MZGW drug-containing serum (MZGW-DS) groups.

In vitro Simulation of SCFAs

SCFAs in the respective groups were prepared to replicate the composition and proportions of acetic, propionic, butyric, valeric, isovaleric, isobutyric, and caproic acids found in the peripheral blood of rats in each group. The pH value was adjusted using a sodium hydroxide solution to fall within the range of 7.2–7.4, thus simulating SCFAs in peripheral blood

Table 2 Primer Sequences

Gene	Forward Primer Sequence (5′-3′)	Reverse Primer Sequence (5′-3′)
ACTB	GTGTGGATTGGTGGCTCTATC	CAGTCCGCCTAGAAGCATTT
P38	CTCATGGTAGCCAGCTAAGAAA	GGCTGTGTCTAATGACCCTATT

https://doi.org/10.2147/DDDT.S482965

as an independent acting factor in vitro. The experimental groups comprised NC-SCFAs, OVX-SCFAs, and MZGW-SCFAs groups.

Cell Counting Kit-8 Assay

RAW264.7 cells were inoculated in 96-well plates at a concentration of 3000 cells/well. After 1–3 days of incubation, the cells were treated with different concentrations of MZGW-DS to determine the safe dosing range using the Cell Counting Kit (CCK)-8 kit (Beyotime, China).

Assessment of OC Differentiation Function: TRAP Staining

RAW264.7 cells were inoculated in 24-well plates at 2×10^4cells/well, and after 24 h, a complete medium (10% FBS+α-MEM+50 ng/mL RANKL) was added for induction for 48 h. Subsequently, rat serum from each group was added. Following this, 200 μL of TRAP dye fixing solution was added to each well and incubated at 4°C for 3 min.The wells were then cleaned with PBS buffer solution (Beyotime), and 200 μL TRAP staining solution was added to each well and incubated at 37°C for 45 min without exposure to light. Finally, the number of $TRAP^+$OCs (≥3 nuclei) in each group was observed and counted under a light microscope.

Determination of OC Bone Resorption Function: Toluidine Blue Staining

The prepared bovine bone slices were placed into a 96-well plate, and RAW264.7 cells were inoculated onto the bone slices at 8×10^3cells/well, with a total medium volume of 200 μL per well. Subsequently, a complete medium (10% FBS +α-MEM+50 ng/mL RANKL) was added for induction for 48 h, followed by the addition of rat serum from each group. After incubation, the bone slices were cleaned using ultrasonic treatment and 1% toluidine blue staining solution (Solarbio, Beijing, China) was added, followed by incubation at room temperature for 10 min.They were then rinsed with pure water. We observed the number and shape of lacunae under the microscope (Leica), and the area of lacunae was calculated using ImageJ software.

Cell Transfection

In this study, the siGPR41 plasmid was initially constructed, and the transfection interference efficiency of the target gene was examined using the WB method. On this basis, the transfection portion of the experiment was divided into four groups: OC+small interfering negative control (siNC), OC+small interfering GPR41 (siGPR41), OC+siNC+MZGW-DS, and OC+siGPR41+MZGW-DS groups. Subsequently, cells were collected for WB assay to verify the differentiation of OCs and the regulation of GPR41, a key factor in the SCFA-GPR41-p38MAPK pathway, by the intervention of MZGW-DS.

Statistical Analysis

SPSS Statistics 23.0 was used for statistical analysis of the data, and GraphPad Prism 8 software was used for drawing statistical graphs. All data were presented as mean ± standard deviation ($\bar{X} \pm SD$). Groups were compared using one-way analysis of variance (ANOVA). Results at $p<0.05$ or $p<0.01$ indicated a significant difference.

Results

Key Active Ingredients in MZGW-H

The total ion flow diagrams in positive and negative ion scanning modes were collected separately, as shown in Figure 1. A total of 10 major blood-entry compounds were isolated and identified and the top three blood components were ferulic acid, L-ascorbic acid and riboflavin (Figure 1, Table 3).

MZGW-H Improved BMD and Bone Microstructure in OVX Rats

To examine the effect of MZGW on the bone microstructure of OVX rats, micro-CT was employed to detect the bone micro-architecture of different treatment groups. Three-dimensional morphometric indices of the femur showed that the

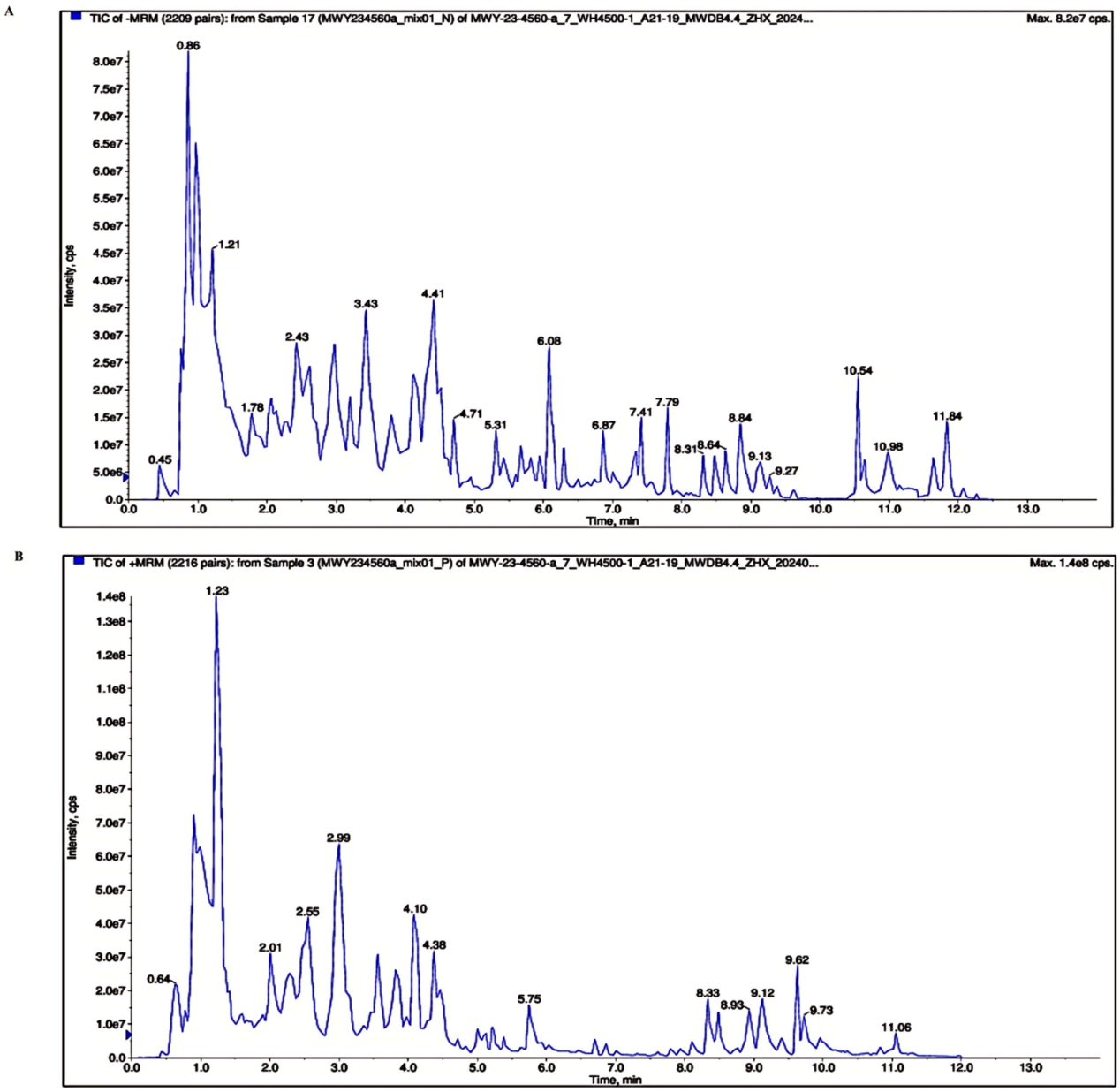

Figure 1 Total ion chromatogram (TIC) diagram of MZGW. (**A**) In positive ion mode. (**B**) In negative ion mode.

bone tissue of the SHAM group was closely arranged and relatively intact (Figure 2A). Compared with the SHAM group, the OVX group exhibited significant loss of femoral bone, characterized by decreased BMD, BV/TV, and Tb.N an increase in Tb.Sp ($p<0.01$; Figure 2B–E). Administration of EV or MZGW high-dose significantly ameliorated the deteriorated all bone microstructure of OVX rats ($p<0.01$), while MZGW low-dose only significantly ameliorated BMD ($p<0.05$). However, compared with OVX rats, MZGW-H group significantly improved BMD than MZGW-L group. Therefore, MZGW-H was more effective than MZGW-L in alleviating bone tissue injury in OVX rats.

Effect of MZGW on Histopathological Changes in Bone Tissue of OVX Rats and Serum Bone Turnover Markers

In the SHAM group, a small medullary cavity was observed, along with trabecular bone that was both full and regular, exhibiting a well-connected net-like pattern (Figure 2F). However, an enlarged medullary cavity with a sparse and

https://doi.org/10.2147/DDDT.S482965

Table 3 UPLC-Q-Exactive-MS of MZGW

No.	Name	Formula	Molecular Weight (Da)	RT(Min)	Mass Error (δ)/ppm	Ionization Model	MS/MS Fragment
1	Betaine	$C_5H_{11}NO_2$	117.08	0.80	12.70	[M+H]+	21,511,996.72
2	L-Ascorbic acid (Vitamin C)	$C_6H_8O_6$	176.03	1.10	0.00	[M-H]-	1,088,162.44
3	Val-Val-Asp	$C_{14}H_{25}N_3O_6$	331.17	1.40	0.30	[M+H]+	209,766.39
4	Thr-Trp	$C_{15}H_{19}N_3O_4$	305.14	2.50	0.00	[M+H]+	394,395.99
5	7R-O-morroniside	$C_{17}H_{26}O_{11}$	406.15	2.60	4.44	[M-H]-	2,464,828.44
6	Methyl gallate	$C_8H_8O_5$	184.04	3.20	25.68	[M-H]-	1,060,845.41
7	Riboflavin (Vitamin B2)	$C_{17}H_{20}N_4O_6$	376.14	3.20	0.00	[M+H]+	6,121,327.83
8	Quercetin-3-O-robinobioside	$C_{27}H_{30}O_{16}$	610.15	3.60	0.00	[M-H]-	836,580.56
9	Ferulic acid	$C_{10}H_{10}O_4$	194.06	4.00	0.00	[M-H]-	5,587,758.72
10	3,24-Dihydroxyolean-12-en-22-one (Soyasapogenol E)	$C_{30}H_{48}O_3$	456.36	11.00	0.00	[M-H]-	325,553.77

disorganized trabecular structure was found in the OVX group. The staining results showed that EV, MZGW-L or MZGW-H treatment ameliorated histopathological alterations in the bone tissue of OVX rats. Our results suggested that the bone microstructure of rats was damaged due to OVX, and the intervention of MZGW-H could effectively alleviate this damage in OVX rats and facilitate bone reconstruction.

The number of $TRAP^+$ OCs in the OVX group was significantly higher than that in the SHAM group, mainly located at the edge of the bone trabeculae (Figure 2G). Compared with that in the OVX group, the number of $TRAP^+$OCs in the MZGW-L group was slightly lower and the number of $TRAP^+$ OCs in the EV and MZGW-H groups was markedly lower. Our results suggested that ovariectomy leads to an increase in the number and activity of OCs in OP rats. The intervention of MZGW-H effectively inhibited the activity and number of OCs in OP rats and reduced bone resorption.

To further confirm the anti-OP effect of MZGW-H, serum bone conversion markers TRAP, BALP, and BGP were tested in OVX rats. Compared with those in the SHAM group, the concentrations of TRAP, BALP, and BGP in the OVX group were significantly increased ($p<0.01$), indicating high bone metabolism after OVX. Compared with those in the OVX group, the concentrations of TRAP, BALP, and BGP in the EV, MZGW-H groups were significantly lower ($p<0.01$, $p<0.05$), while MZGW-L groups had no significant change. Compared with those in MZGW-L groups, MZGW-H groups had markedly changed. ($p<0.05$, $p<0.01$; Figure 2H, I and J). Therefore, MZGW-H was more effective than MZGW-L in alleviating serum bone conversion markers in OVX rats. Based on the above results, it can be preliminarily concluded that MZGW-H was more effective than MZGW-L. Therefore, we explored the mechanism by which MZGW improves bone damage, and all the following MZGW referred to MZGW-H.

Effect of MZGW-H on Relative Protein Expression Levels of Bone Resorption-Related Indicators (CTSK and NFATc1), SCFAs and SCFA-GPR41-p38MAPK Signaling Pathway in OVX Rats

Compared with SHAM group, OVX group significantly increased the protein levels of CTSK and NFATc1 ($p<0.01$; Figure 3A–C). MZGW-H treatment significantly reduced the protein levels of CTSK and NFATc1 ($p<0.01$, $p<0.05$; Figure 3A–C). Thus, MZGW-H treatment could improve bone metabolism to a certain extent by reversing the expression of bone metabolism markers in serum and tibia.

SCFAs are effective regulators of OC metabolism and bone homeostasis, playing a key role in the prevention and treatment of OP. To verify the effect of MZGW-H on the metabolism of SCFAs, GC-MS was used to determine the concentration of serum SCFAs. Serum SCFAs levels significantly decreased after OVX ($p<0.05$; Figure 3D), while the decreased levels were significantly increased after EV and MZGW-H intervention ($p<0.01$, $p<0.05$). Additionally, EV and MZGW-H reversed the trend of change in serum SCFAs caused by OVX.

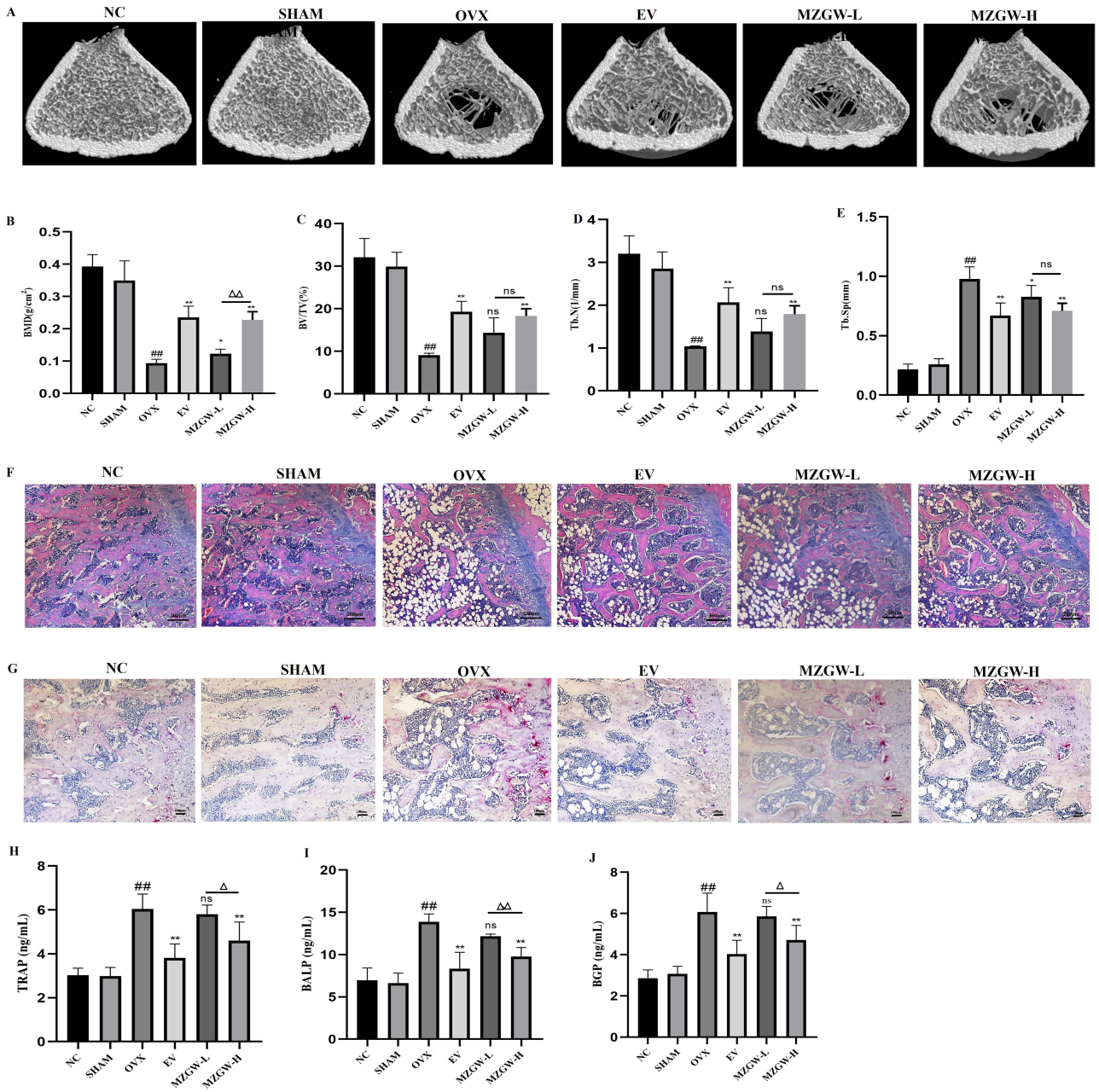

Figure 2 Effect of MZGW-L and MZGW-H on bone microstructure change and serum indicators in OVX rats. (**A**) Scanning images of bone microstructure. (**B**) Bone mineral density (BMD). (**C**) Bone volume/tissue volume (BV/TV). (**D**) Trabecular number (Tb.N). (**E**) Trabecular separation (Tb.Sp). Data are expressed as mean ±SD, n=6. $^{\#}p<0.05$ and $^{\#\#}p<0.01$ vs the SHAM group; $^{*}p<0.05$ and $^{**}p<0.01$ vs the OVX group; $^{\Delta\Delta}p<0.01$ vs the MZGW-L group; ns means no significance. (**F**). Morphological changes in bone histopathology (HE staining, scale bar=200 μm). (**G**) Morphological changes in bone histopathology (TRAP staining, scale bar=100 μm). (**H**) Changes in serum tartrate-resistant acid phosphatase (TRAP) level. (**I**) Changes in serum bone alkaline phosphatase (BALP) level. (**J**) Changes in serum bone gamma-carboxyglutamic acid-containing protein (BGP) level. Data are expressed as mean ±SD, n=6. $^{\#\#}p<0.01$ vs the SHAM group; $^{*}p<0.05$ and $^{**}p<0.01$ vs the OVX group; $^{\Delta}p<0.05$ and $^{\Delta\Delta}p<0.01$ vs the MZGW-L group.

Furthermore, the relative expression of GPR41 and p38 in OVX rat tibia was assessed to determine the effects of MZGW on the SCFA-GPR41-p38MAPK signaling pathway. The protein levels of GPR41 in the tibia were markedly elevated by treatment with MZGW-H compared with that in the OVX group (Figure 3E and F). Additionally, the administration of MZGW-H upregulated GPR41 protein. However, p38 exhibited an expression trend opposite to that of GPR41 protein. (Figure 3G–I). Moreover, NFATc1 and CTSK showed protein expression trends similar to that of p38 (Figure 3A–C). Collectively, MZGW-H treatment can attenuate OP by regulating the SCFA-GPR41-p38MAPK signaling pathway.

https://doi.org/10.2147/DDDT.S482965

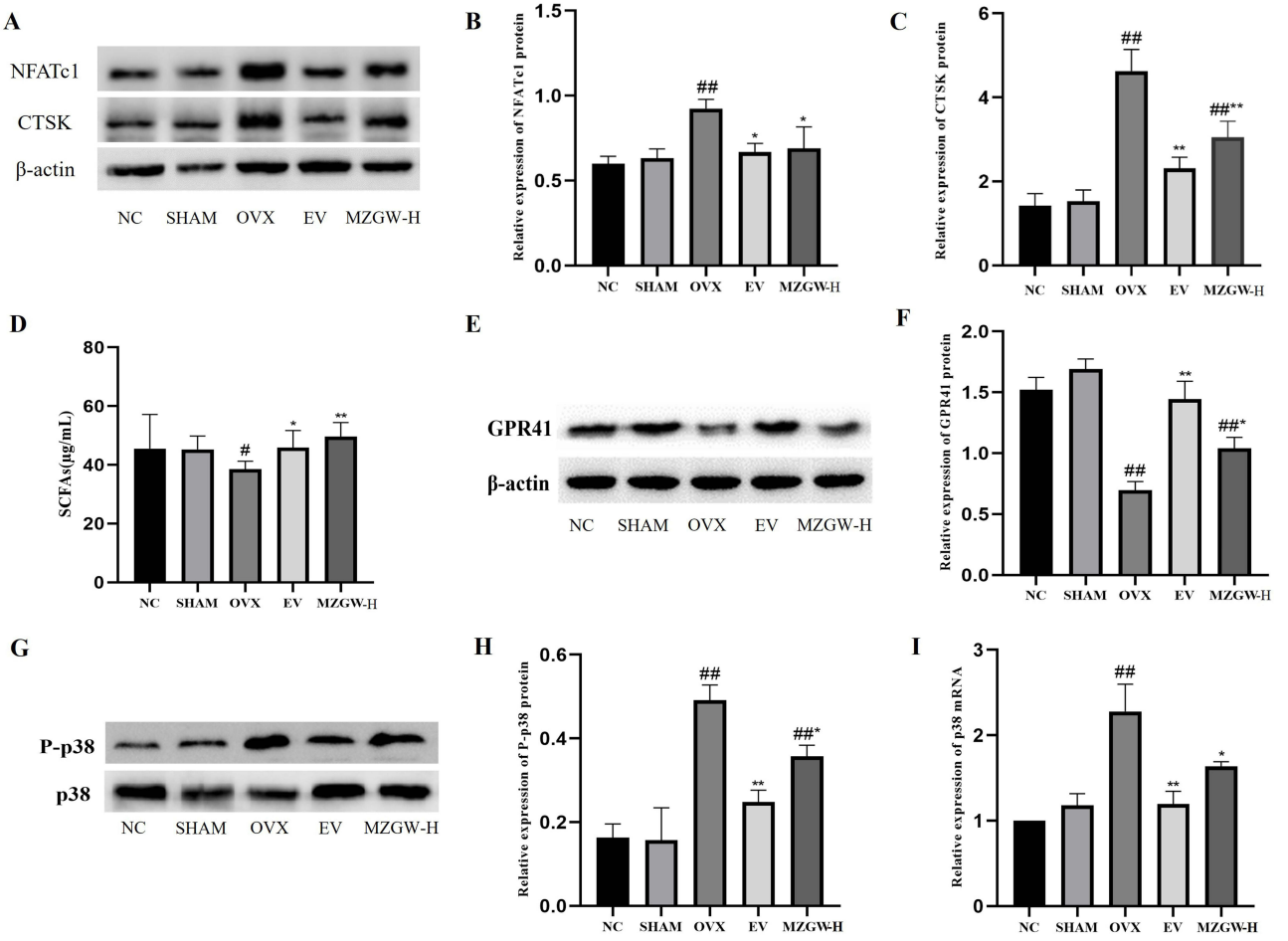

Figure 3 Effect of MZGW on serum SCFA level and the relative expression of tibia CTSK, NFATc1, GPR41, and p-p38 proteins in OVX rats. (**A**) Western blot image of NFATc1 and CTSK protein expression. (**B**) Relative protein expression of NFATc1. (**C**) Relative protein expression of CTSK. (**D**) Changes in the total serum SCFA levels per group. (**E**) Western blot image of GPR41 protein expression. (**F**) Relative protein expression of GPR41. (**G**) Western blot image of p-p38 and p38 protein expression. (**H**) Relative protein expression of p-p38. (**I**) Relative mRNA expression of p38 examined using quantitative reverse transcription PCR (qRT-PCR). Data were expressed as mean ± SD, n=6. $^{\#}p<0.05$ and $^{\#\#}p<0.01$ vs the SHAM group; $^{*}p<0.05$ and $^{**}p<0.01$ vs the OVX group.

Effect of MZGW-H on Intestinal Flora Diversity in OVX Rats

We used 16S rRNA gene sequencing to assess changes in intestinal flora. Results of operational taxonomic unit (OTU) analysis revealed a total of 30,922 OTUs in five groups, with 5,080 OTUs common to all groups. The NC group exhibited 9,172 unique OTUs, of which 4,092 were exclusive to this group. Similarly, the SHAM group had 11,171 OTUs, with 6,091 unique to it. The OVX group exhibited 11,231 OTUs, with 6,151 being unique to this group. The EV group presented 10,326 OTUs, with 5,246 being exclusive to this group. Lastly, the MZGW-H group had 9,342 OTUs, with 4,262 exclusive to it (Figure 4A).Taken together, the results indicated that OVX can lead to changes in relative OTU abundance, and MZGW-H can reverse these changes.

The dilution curve was used to observe the adequacy of sample size, with a smooth end of the dilution curve indicating that the quantity of sequencing data is reasonable (Figure 4B). Each curve in Figure 4C–F represents a sample of intestinal flora data, and the smooth end of the dilution curve indicates reasonable sequencing data quantity for each sample. Alpha diversity analysis, including the Chao1 (Figure 4G), Observed_species (Figure 4H), PD_whole_tree (Figure 4I) and Shannon (Figure 4J), revealed an increase in overall microbial diversity in the OVX group compared with that in the SHAM group ($p<0.01$, $p<0.05$). However, MZGW-H administration significantly prevented the aforementioned parameter indices ($p<0.01$). *Bacteroidetes*, *Firmicutes*, and *Proteobacteria* were the dominant phyla in each group (Figure 4K and L) at the phylum level (Figure 4M–Q). The *Firmicutes* to *Bacteroidetes* ratio (F/B ratio) is used as a common parameter to assess the impact of intestinal flora on various diseases. We observed a significant increase in the

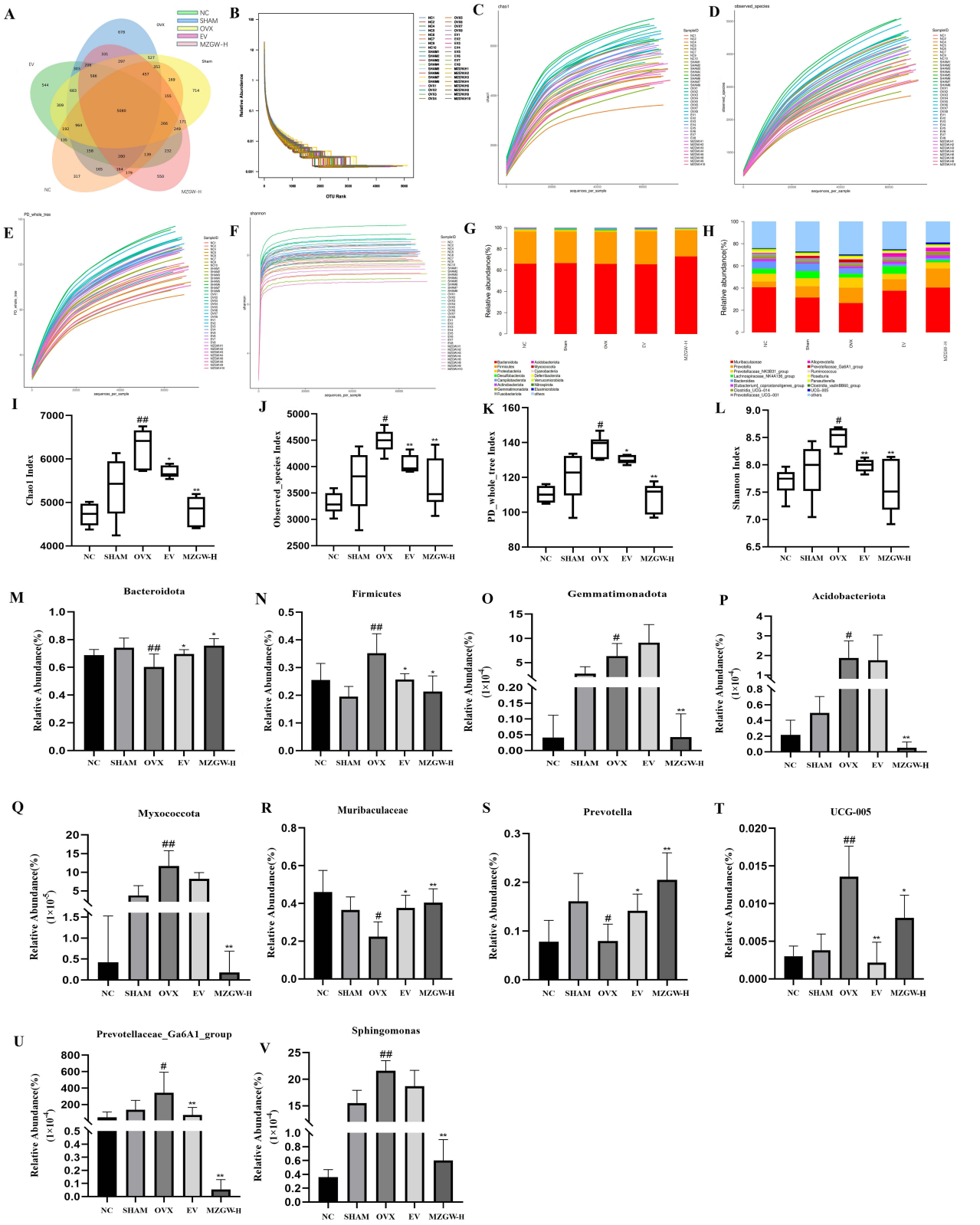

Figure 4 Effect of MZGW-H on intestinal flora in OVX rats and prediction of potential metabolic functions of intestinal flora. (**A**) Venn diagrams of OTUs of intestinal flora per group. Green, blue, yellow, pink, and Orange ellipses represent the NC, SHAM, OVX, EV, and MZGW-H groups, respectively. (**B**) Rank-abundance curves of intestinal flora per group. (**C–F**) Dilution curves of alpha diversity index of intestinal flora per group. (**G**) Effect of MZGW-H on Chao1 index. (**H**) Effect of MZGW-H on observed species index. (**I**) Effect of MZGW-H on PD whole tree index. (**J**) Effect of MZGW-H on Shannon index. (**K**) Histogram of relative abundance of intestinal flora at the phylum level per group. (**L**) Horizontal and vertical coordinates represent different groups and relative abundance, respectively, while different colors indicate different species. (**M–Q**) Histograms of differential intestinal flora at the phylum level. (**R–V**) Histograms of differential intestinal flora at the genus level. Data are expressed as mean ± SD, n=6. $^{\#}p<0.05$ and $^{\#\#}p<0.01$ vs the SHAM group; $^{*}p<0.05$ and $^{**}p<0.01$ vs the OVX group.

https://doi.org/10.2147/DDDT.S482965

F/B ratio in the OVX group compared with that in the SHAM group, whereas MZGW-H reversed this alteration. At the genus level (Figure 4R–V), the relative abundance of *Muribaculaceae* was lower ($p<0.05$; Figure 4R) in the OVX group than in the SHAM group, whereas that of *Prevotellaceae_Ga6A1_group* and *UCG-005* were higher ($p<0.01$, $p<0.05$; Figure 4S and T). However, the MZGW-H treatment reversed these alterations in the aforementioned intestinal flora.

Screening of Optimal Concentration of MZGW-DS

However, the number of $TRAP^+$ cells in the 2.5% and 5% MZGW-DS groups was substantially lower than that in the OVX-S group ($p<0.01$). Additionally, the number of $TRAP^+$ cells in the 5% MZGW-DS group was lower than that in the 2.5% MZGW-DS group ($p<0.05$; Figure 5A and B). In this study, the CCK-8 method was used to evaluate the activity of RAW264.7 cells treated with 0–20% MZGW-DS over three periods: 24 h, 48 h, and 72 h. The results indicated that 0–5% MZGW-DS exhibited no toxicity to RAW264.7 cells (Figure 5C–E). TRAP staining was used to further determine the final concentration of MZGW-DS. After TRAP staining, the number of $TRAP^+$ cells with ≥3 nuclei increased significantly in the OVX-S group ($p<0.01$).

Effect of Serum and Peripheral Blood Concentration of SCFAs on the Differentiation of OCs in Counterpart Groups

To compare the effects of SCFAs and serum on OC differentiation, we investigated the effects of peripheral blood concentrations of SCFAs and serum on OC differentiation in corresponding groups of rats with TRAP staining. The number of $TRAP^+$OCs significantly increased in the OVX-S group compared to the NC-S group ($p<0.01$; Figure 6A and B). However, the number of $TRAP^+$OCs significantly decreased in the MZGW-DS group compared to the OVX-S group ($p<0.01$). Additionally, the effects of peripheral blood concentration of SCFAs on the number of $TRAP^+$OCs in the corresponding groups showed a similar trend ($p<0.01$). Compared with the MZGW-SCFAs group, the MZGW-DS group exhibited a significant reduction in the number of $TRAP^+$ cell ($p<0.01$). The above experimental results indicated that peripheral blood concentration of SCFAs inhibited the OCs differentiation, but its inhibitory effect was weaker than that of MZGW-DS.

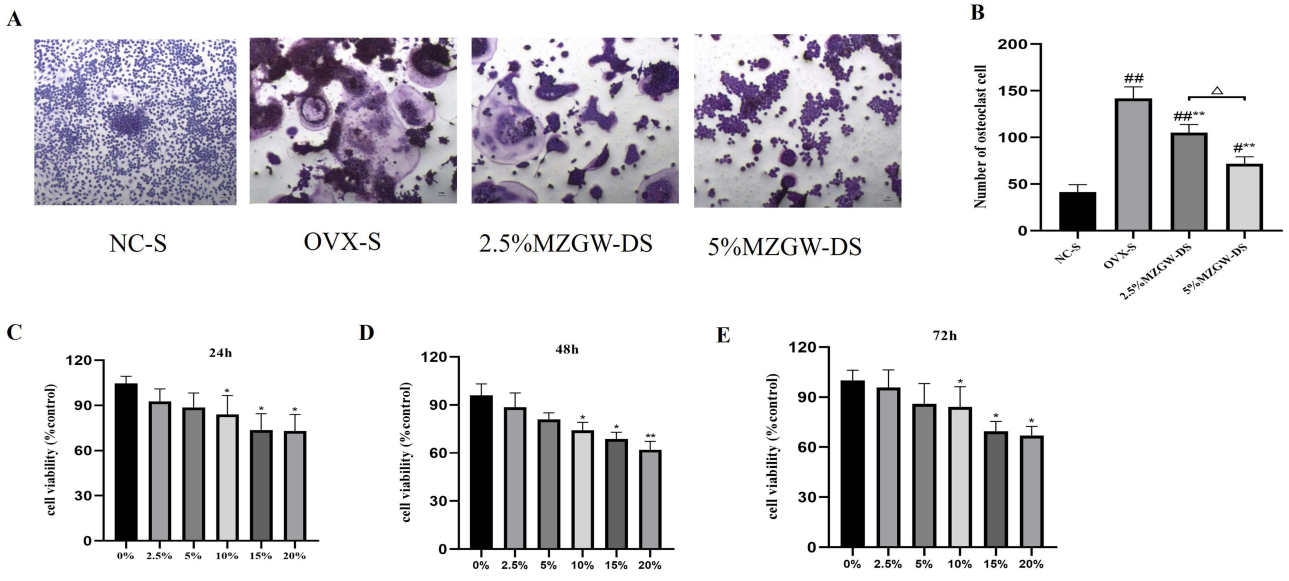

Figure 5 MZGW-DS inhibited OC differentiation and bone resorption. (**A**) Representative images of TRAP-stained OCs at different concentrations of MZGW-DS. Differentiation of osteoclasts in each group (scale bar=100 μm). (**B**) Quantitative statistics of OC number per bone surface. (**C–E**) Viability of RAW264.7 cells treated with different concentrations of MZGW-DS for 24 h, 48 h, and 72 h. Data are expressed as mean ±SD, n=5. *$p<0.05$ and **$p<0.01$ vs Control. Data are expressed as mean ± SD, n = 5. $^{\#}p<0.05$ and $^{\#\#}p<0.01$ vs the NC-S group; **$p<0.01$ vs the OVX-S group; $^{\Delta}p<0.05$ vs the 2.5% MZGW-DS group.

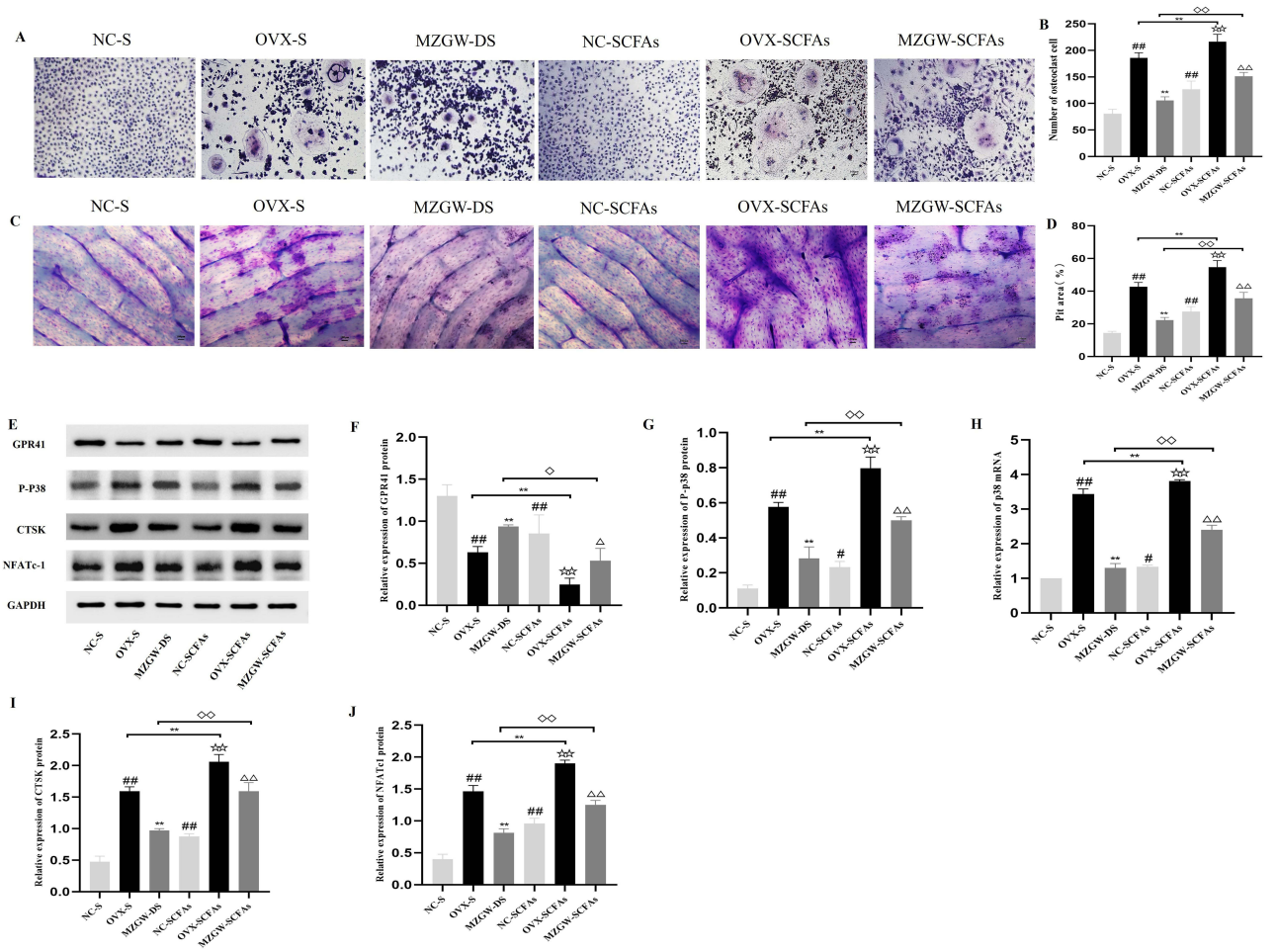

Figure 6 SCFAs inhibited osteoclast differentiation and decrease the expression of mRNA and proteins associated with the SCFA-GPR41-p38MAPK signaling pathway. (**A**) Representative images of TRAP-stained osteoclasts depicting osteoblast differentiation in each group (scale bar=100 μm). (**B**) Quantitative statistics of osteoclast number (n=6). (**C**) Representative images of toluidine blue-stained osteoclasts in each group depicting bone resorption function. Differentiation of osteoblasts in each group (scale bar=100 μm). (**D**) Measurement of the area of bone resorption lacunae using Image-pro-plus 6.0 software. Data are expressed as mean ± SD, n=6. (**E**) Western blot image of GPR41, p-p38, CTSK, and NFATc1 protein expression. (**F**) Relative protein expression of GPR41. (**G**) Relative protein expression of p-p38. (**H**) Relative mRNA expression of p38. (**I**) Relative protein expression of CTSK. (**J**) Relative protein expression of NFATc1. Data are expressed as mean ± SD, n=6. $^{\#}p<0.05$ and $^{\#\#}p<0.01$ vs the NC-S group; $^{**}p<0.01$ vs the OVX-S group; $^{\diamond}p<0.05$ and $^{\diamond\diamond}p<0.01$ vs the MZGW-DS group; $^{\star\star}p<0.01$ vs the NC- SCFAs group; $^{\Delta}p<0.05$ and $^{\Delta\Delta}p<0.01$ vs the OVX-SCFAs group.

To compare the effects of SCFAs and serum on the area of bone resorption, we investigated the effects of peripheral blood concentrations of SCFAs and serum on the area of bone resorption in corresponding groups of rats with toluidine blue staining. The area of bone resorption area were significantly increased in the OVX-S group compared to the NC-S group ($p<0.01$; Figure 6C and D). However, the area of bone resorption were significantly decreased in the MZGW-DS group compared to the OVX-S group ($p<0.01$). However, Compared with the MZGW-SCFAs group, the MZGW-DS group exhibited a significant reduction in the area of bone resorption ($p<0.01$). The above experimental results indicated that peripheral blood concentration of SCFAs inhibited the area of bone resorption, but its inhibitory effect was weaker than that of MZGW-DS.

Effect of MZGW-DS on the SCFA-GPR41-p38MAPK Signaling Pathway

The relative expression of GPR41 and p38 in RAW264.7 cells was assessed to determine the effects of MZGW on the SCFA-GPR41-p38MAPK signaling pathway. The protein levels of GPR41 in the cells were markedly elevated by treatment with MZGW-DS compared with that in the OVX-S group (Figure 6E and F). Additionally, the administration of MZGW-DS upregulated GPR41 protein. However, p38 exhibited an expression trend opposite to that of GPR41 at both the gene and protein levels (Figure 6G and H). Moreover, NFATc1 and CTSK showed protein expression trends similar to that of p38 (Figure 6E, I and J). Collectively, MZGW-DS could attenuate OP by regulating the SCFA-GPR41-p38MAPK signaling pathway.

https://doi.org/10.2147/DDDT.S482965

Effect of MZGW-DS on OC Differentiation and the SCFA-GPR41-p38MAPK Signaling Pathway Following GPR41 Knockdown

Interference Through Knockdown of GPR41

After knocking down the expression level of GPR41 via liposome transfection, three higher-scoring sequences were selected for synthesis: si187, si495, and si966. The WB method was used to detect the transfection efficiency of each fragment. Compared with that in the OC+siNC group, the protein expression of GPR41 was significantly downregulated in the OC+si187, OC+si495, and OC+si966 groups, particularly evident in the OC+si495 group (p<0.01; Figure 7A and B). These experimental results indicated the successful knockdown of GPR41 in RAW264.7 cells.

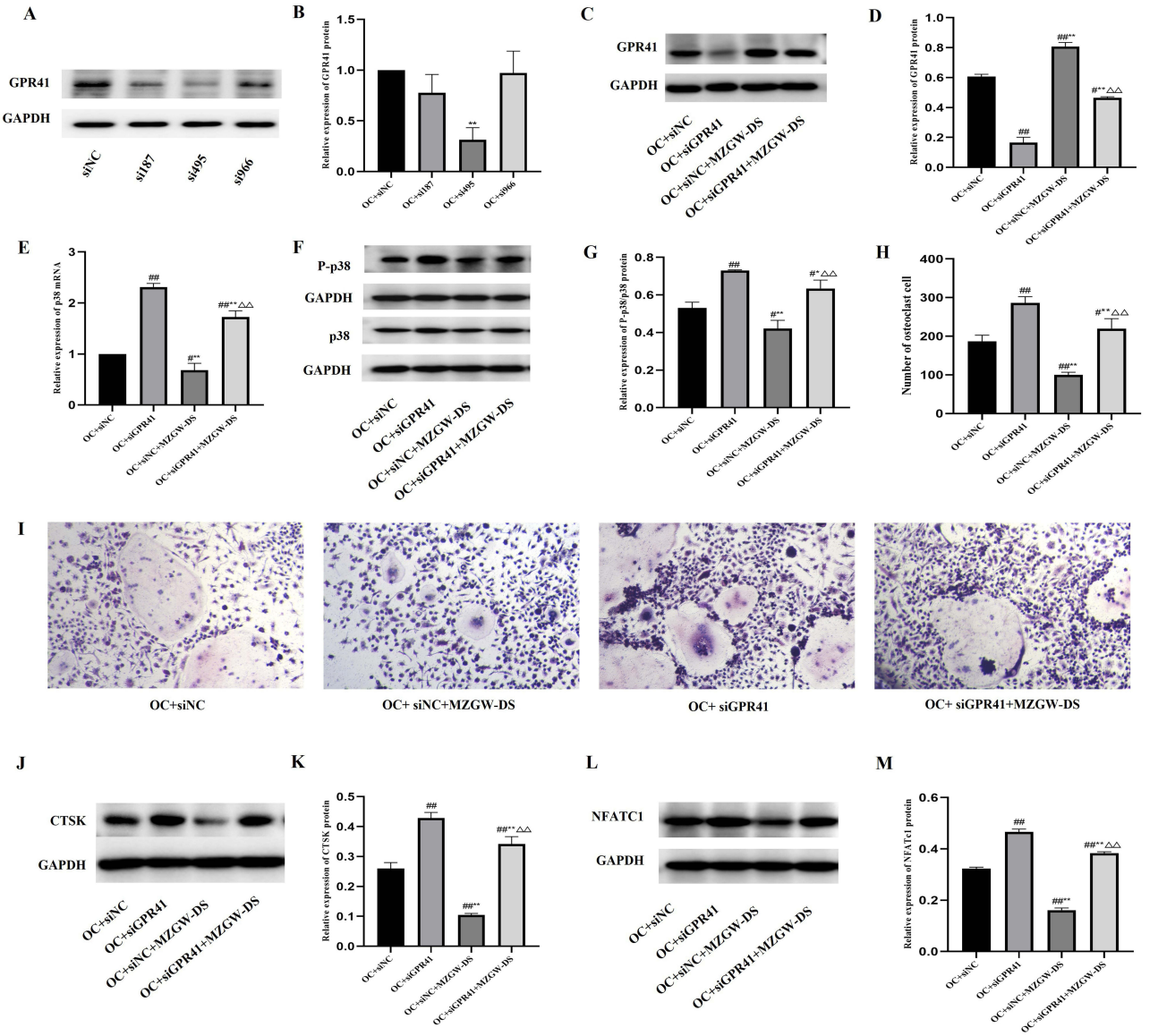

Figure 7 Knockdown of the GPR41 gene, a key receptor for SCFAs binding in the SCFA-GPR41-p38MAPK pathway, did not reverse osteoclast-induced bone destruction by MZGW drug-containing serum (MZGW-DS). (**A**) Transfection efficiency of knocked down GPR41 protein detected using Western blotting. (**B**) Relative protein expression of GPR41. Data are expressed as mean ± SD, n=6. *p<0.05 and **p<0.01 vs the OC+siNC group. (**C**) Western blot image depicting GPR41 protein expression upon knockdown of the GPR41 gene. (**D**) Relative protein expression of GPR41. (**E**) Relative expression of p38mRNA in osteoclasts in each group. (**F**) Western blot image depicting p-p38 and p38 protein expression upon knockdown of the GPR41 gene. (**G**) Relative protein expression of p-p38 and p38. (**H**) Quantitative statistics of osteoclast number (n=6). (**I**) Representative images of TRAP-stained osteoclasts in each group (scale bar=100 μm) upon knockdown of the GPR41 gene. (**J**) Western blot image of CTSK protein. (**K**) Relative protein expression of CTSK. (**L**) Western blot image of NFATc1 protein. (**M**) Relative protein expression of NFATc1. Data are expressed as mean ± SD, n=6. $^{\#}p$<0.05 and $^{\#\#}p$<0.01 vs the OC+siNC group; *p<0.05 and **p<0.01 vs the OC+siGPR41 group; $^{\triangle\triangle}p$<0.01 vs the OC+siNC+MZGW-DS group.

 https://doi.org/10.2147/DDDT.S482965

Effect of MZGW-DS on OC Differentiation After Knockdown of GPR41

The number of $TRAP^+$ cells significantly increased in the OC+siGPR41 and OC+siGPR41+MZGW-DS groups after GPR41 knockdown ($p<0.01$, $p<0.05$), whereas it substantially decreased in the OC+siNC+MZGW-DS group ($p<0.01$). Compared with that in the OC+siGPR41 group, the number of $TRAP^+$ cells in the OC+siNC+MZGW-DS and OC +siGPR41+MZGW-DS groups significantly decreased ($p<0.01$). However, the number of $TRAP^+$ cells in the OC +siGPR41+MZGW-DS group significantly increased compared with that in the OC+siNC+MZGW-DS group ($p<0.01$; Figure 7C and D).

Effect of MZGW-DS on the SCFA-GPR41-p38MAPK Signaling Pathway After Knockdown of GPR41

The relative mRNA levels of p38 were markedly increased after GPR41 knockdown ($p<0.01$). Compared with the OC +siGPR41 group, the OC+siNC+MZGW-DS and OC+siGPR41+MZGW-DS groups exhibited significantly decreased in the relative expression of p38 mRNA ($p<0.01$). Additionally, the relative expression of p38mRNA in the OC+siGPR41 +MZGW-DS group was substantially increased compared with that in the OC+siNC+MZGW-DS group ($p<0.01$; Figure 7E). The administration of MZGW-DS decreased the protein level of p-p38 (Figure 7F and G). However, the relative protein levels of GPR41 exhibited an expression trend opposite to that of p-p38 (Figure 7C and D). Moreover, the TRAP staining exhibited similar trends as bone absorption indicators (Figure 7H and I) and the protein expression of CTSK and TRAP showed similar trends as that of p-p38 (Figure 7J–M). These results indicate the inhibition of the SCFA-GPR41-p38MAPK signaling pathway after GPR41 knockdown, suggesting that this signaling pathway is a critical mechanism for MZGW treatment in relieving OP.

Discussion

Intestinal flora affects bone metabolic homeostasis.[23] SCFAs, the primary metabolites of intestinal flora, inhibit bone loss and exert a bone protective effect.[24] In the present study, we investigated the anti-OP effects of MZGW-H. MZGW-H restored the changes in the intestinal flora and its metabolite SCFAs, reduced OVX-induced bone loss in vivo, and inhibited OC differentiation in vitro. This modulation occurred through the regulation of the SCFA-GPR41-p38MAPK signaling pathway. Additionally, transfected with GPR41 further confirmed the mechanism of action of MZGW-H.

In this study, we demonstrated that MZGW-H improved bone tissue structure and increased bone mass in OVX rats. Specifically, the levels of BMD, BV/TV, and Tb.N were significantly increased in the MZGW-H group, whereas the levels of Tb.Sp were significantly decreased, indicating that MZGW-H alleviated changes in the OVX-induced OP rat model. Based on previous reports, TRAP (OC-specific marker), BALP (osteoblast-specific marker), and BGP (osteoblast-specific marker) were selected as serum markers reflecting bone turnover. These markers can indicate the level of bone metabolism in each group of rats.[21,22] In our study, we elucidated that the expression levels of TRAP, BALP, and BGP were significantly decreased in the MZGW-H group compared with those in the OVX group. Moreover, we compared the changes in bone microarchitecture, HE, TRAP and serum bone turnover markers between the MZGW-H and MZGW-L groups. This finding suggested that MZGW-H could reduce the level of bone turnover, inhibit OC formation, and regulate bone remodeling and MZGW-H is more effective than MZGW-L. Therefore, we explored the mechanism by which MZGW improves bone damage, and all the following MZGW referred to MZGW-H.

Moreover, we observed that MZGW-H promoted the homeostasis of intestinal flora, increased the content of SCFAs, and regulated the type and proportion of SCFAs in OVX rats. Regarding intestinal flora, the OVX group exhibited the highest abundance, whereas the MZGW-H group had significantly lower abundance and diversity of intestinal flora than the OVX group. However, previous study results on the relationship between intestinal flora and OP in denuded rats showed that the abundance and diversity of intestinal flora were lower in the OVX group than in the SHAM group. Furthermore, the abundance and diversity of intestinal flora in the medicated group were higher than those in the OVX group, which is contrary to the results of the present study. Combined with alpha diversity index analysis, we inferred that OVX caused changes in the intestinal flora, and MZGW-H reversed these changes in OVX rats to some extent. Furthermore, the F/B ratio showed an upward trend in the OVX group, suggesting changes in the structure and function of intestinal flora after OVX. Statistically significant differences in the intestinal flora at the phylum and genus levels were concentrated in low abundance flora. This phenomenon may be due to the multifactorial nature of OP, which is

a chronic progressive disease. Specific high abundance flora might be undergoing changes in the occurrence of OP due to the complex and variable intestinal environment, where the flora interact with each other. Under specific conditions or the influence of functionally similar flora, the change in high abundance flora occurs temporarily before reaching equilibrium. Additionally, the limited sample size of this study may have contributed to this observation. Most differential species belonging to the genera *Rumenococci, Bacteroides*, and *Prevotella*can produce SCFAs and exert anti-inflammatory effects.[25,26] The population of *Rumenococci* was elevated in the MZGW group, and the population of *Bacteroides* was significantly decreased in the OVX group, whereas MZGW-H was able to reverse this alteration. *Prevotella* levels were significantly elevated in the MZGW-H group and contributed significantly to the differences in intestinal flora. Studies have confirmed that changes in SCFAs serve as biomarkers of bone metabolic activity, and supplementation of probiotics or prebiotics can alter the structure of intestinal flora to regulate SCFAs and improve bone mass.[23,27] In our study, changes in the content and proportion of SCFAs in the OVX group were reversed by MZGW-H.

The results of TRAP and toluidine blue staining revealed a significant increase in the number of OCs and the area of bone resorption traps in the OVX-S group, indicating that OVX rat serum could enhance OC proliferation and bone resorption. This finding is consistent with the observed decrease in bone mass and increase in bone resorption in vivo following OVX in rats. Moreover, these indicators improved after treatment with MZGW-DS, demonstrating a trend consistent with in vivo experiments.

The SCFA-GPR41-p38MAPK signaling pathway may represent one of the key pathways contributing to the anti-OP effect of MZGW-H. Upon activation of the RANKL-stimulated MAPK signaling cascade, a series of downstream transcription factors are induced.[28,29] RANKL induces the activation of the c-FOS pathway, leading to the self-amplification of the OC transcription factor NFATc1;[30] thus, c-FOS and NFATc1 are key transcription factors for OC formation.[31,32] p38 directly enhances the mRNA expression of NFATc1, promoting the mRNA expression of CTSK and thereby promoting OC proliferation.[33] In animal experiments, we observed that the relative mRNA and protein expression of p38 in bone increased, whereas the relative expression of GPR41 decreased in OVX rats. MZGW-H administration reversed these changes. The results indicate that MZGW-H may activate the SCFA-GPR41-p38MAPK signaling pathway by increasing GPR41 expression and downregulating the p38 phosphorylation level to regulate bone homeostasis. To investigate the mechanism by which SCFAs inhibiting OC differentiation, we performed in vitro simulations based on the ratios and contents of SCFAs in the peripheral blood of different rat groups from the in vivo experiments. We applied qRT-PCR and WB methods to determine the relative expression of mRNA and protein associated with key pathway factors. The results indicated that SCFAs in the peripheral blood of the MZGW group increased GPR41 expression and negatively regulated the p38MAPK signaling pathway. This resulted in the down-regulation of the OC-related genes and proteins (NFATc1 and CTSK) and effective inhibition of OC differentiation and bone resorption function. Additionally, we observed that the anti-OP effect of MZGW drug-containing serum was superior to that of its SCFAs. This finding suggested that MZGW-H might affect bone metabolism not only through this pathway but also through other mechanisms involving various active ingredients and multiple target points of action. Finally, we investigated the effects of GPR41 knockdown, which is the key target for SCFA binding, on the inhibition of OC differentiation in the MZGW-DS group. The results revealed that knocking down GPR41 in theOC+siGPR41+ MZGW-DS group influenced the effect of the SCFA-GPR41-p38MAPK signaling pathway in the OC culture system. After knocking down GPR41, the number of $TRAP^+$ cells significantly increased. GPR41 protein, a key expression factor of the signaling pathway, was significantly downregulated, indicating inhibition of the SCFA-GPR41-p38MAPK signaling pathway. However, MZGW-DS reversed these changes.

The administration of MZGW-H effectively mitigated bone loss in OVX rats. This could be attributed to the abundant presence of multiple active ingredients identified by UPLC-MS/MS, including ferulic acid, vitamin C, betaine, quercetin, monensin, methyl gallate, and valine-valine-aspartic acid in MZGW. Several studies have confirmed that these active ingredients show significant anti-OP effects through various mechanisms. Ferulic acid[32] and vitamin C,[33] as active components of ripened yam, inhibit osteoclastogenesis through the SIRT1/NF-κB and Wnt/β-catenin/ATF4 signaling pathways, respectively, thus protecting against OP in rats. Betaine, an alkaloid from matrimony vine, enhances osteoblast expression and bone formation via multiple signaling pathways, including calcium flow, ERK activation, and IGF-1 production, thereby exerting an anti-OP effect.[34] The terpene oleanolic acid, the active ingredient in Huai Niu Knee,

alleviates glucose metabolism disorders and enhances molecular transport and lipid metabolism in glucocorticoid-induced OP rats.[35] The flavonoid quercetin, the active constituent of *Cuscuta*, promotes osteogenic differentiation of mesenchymal stem cells, thereby alleviating OP.[36] Monosaccharide glycosides derived from *Cornus officinalis* promote increased osteoblast differentiation and decreased OC differentiation, thereby inhibiting OVX-induced OP pathogenesis in mice.[37] The peptide valine-valine-aspartic acid, an active ingredient in tortoise and deer antler gums, has been linked to fibrous network formation, inhibition of OC differentiation, and OP prevention.[38] Therefore, the anti-OP effect of MZGW-H may result from the synergistic effect of various components.

The limitations of the research were the small sample size and lacked validation in populations. Moreover, the intestinal metabolism was complex and variable, so the study of intestinal flora was not detailed and in-depth enough. The following experiments can investigate which specific acids in total SCFAs are affected by MZGW-H thereby improving osteoporosis. In the prospective time, based on MZGW-H, we can develop standardized and highly controllable modern traditional Chinese medicine preparations to provide a novel therapeutic strategy for improving osteoporosis in patients and provide the scientifical evidence for the clinical application of MZGW-H.

Conclusion

In this study, we systematically explored the therapeutic effect of MZGW-H on OP using an OVX rat model and an OC model. MZGW-H was found to effectively alleviate OP by enhancing intestinal flora diversity, increasing SCFAs content, and inhibiting OC differentiation. Additionally, the SCFA-GPR41-p38MAPK signaling pathway may be one of the key pathways for MZGW-H to exert anti-OP effect. Thus, these findings provide an experimental basis for MZGW-H in the treatment of OP.

Abbreviations

OP, Osteoporosis; MZGW-DS, MZGW drug-containing serum; MZGW, Modified Zuo Gui Wan; OVX, Ovariectomy; OC, Osteoclast; SCFAs, short-chain fatty acids; GPCR, Gi/o protein-coupled receptor; MAPK, Mitogen-activated protein kinases; ERK, Extracellular signal-regulated kinase; JNK, c-Jun N-terminal kinase; BMD, Bone mineral density; TRAP, Tartrate-resistant acid phosphatase; BALP, Bone Alkaline Phosphatase; BGP, Bone-y-Carboxyglutamic Acid-Containing protein; EV, Estradiol valerate; OPG, Osteoprotegerin; NFATc1, Nuclear Factor of Activated T Cells; CTSK, Cathepsin K; P38 MAPK, Protein 38 mitogen-activated protein kinases.

Data Sharing Statement

The raw data supporting the conclusions of this article will be made available by the authors, without undue reservation.

Consent for Publication

All authors agreed to the publication of this manuscript.

Author Contributions

All authors made a significant contribution to the work reported, whether that is in the conception, study design, execution, acquisition of data, analysis and interpretation, or in all these areas; took part in drafting, revising or critically reviewing the article; gave final approval of the version to be published; have agreed on the journal to which the article has been submitted; and agree to be accountable for all aspects of the work.

Funding

This work was supported by the National Natural Science Foundation of China (grant number: 82074297), CACMS Innovation Fund (grant number: CI2021A00107).

Disclosure

The authors declare that the research was conducted in the absence of any commercial or financial relationships that could be construed as a potential conflict of interest.

References

1. Li Y, Shi Z, Feng S, et al. Systematic analysis of miRNAs in patients with postmenopausal osteoporosis. *Gynecol Endocrinol*. 2020,Nov,;36 (11):997–1001. doi:10.1080/09513590.2020.1785420
2. Compston JE, McClung MR, Leslie WD. Osteoporosis. *Lancet*. 2019,Jan 26;393(10169):364–376. doi:10.1016/S0140-6736(18)32112-3
3. Zhang Z, Chen Y, Xiang L, Wang Z, Xiao GG, Hu J. Effect of curcumin on the diversity of gut microbiota in ovariectomized rats. *Nutrients*. 2017;9 (10):1146. doi:10.3390/nu9101146
4. Ai T, Shang L, Li B, Li J, Qin R. Konjac Oligosaccharides alleviated ovariectomy-induced bone loss through gut microbiota modulation and Treg/ Th17 regulation. *J Agri Food Chem*. 2024;72(14):7969–7979. doi:10.1021/acs.jafc.4c00281
5. Shen G, Shang Q, Zhang Z, et al. Zuo-Gui-Wan aqueous extract ameliorates glucocorticoid-induced spinal osteoporosis of rats by regulating let-7f and autophagy. *Front Endocrinol*. 2022;13:878963. doi:10.3389/fendo.2022.878963
6. Liu F, Tan F, Tong W, et al. Effect of Zuoguiwan on osteoporosis in ovariectomized rats through RANKL/OPG pathway mediated by β2AR. *Biomed Pharmacothe*. 2018;103:1052–1060. doi:10.1016/j.biopha.2018.04.102
7. Li W, Liu Z, Liu L, et al. Effect of Zuogui pill and Yougui pill on osteoporosis: a randomized controlled trial. *J Trad Chin Med*. 2018;38(1):33–42.
8. Dong Y, Cheng H, Liu Y et al. Red yeast rice ameliorates high-fat diet-induced atherosclerosis in Apoe-/-mice in association with improved inflammation and altered gut microbiota composition. *Food Funct*. 2019, ;10(7):3880–3889 doi:10.1039/c9fo00583h.
9. Yang H, Pan R, Wang J, et al. Modulation of the gut microbiota and liver transcriptome by red yeast rice and monascus pigment fermented by purple monascus SHM1105 in rats fed with a high-fat diet. *Front Pharmacol*. 2020;11:599760. doi:10.3389/fphar.2020.599760
10. Zhou H, Liu W, Lv Y, et al. Supplementation with natto and red yeast rice alters gene expressions in cholesterol metabolism pathways in ApoE(-/-) mice with concurrent changes in gut microbiota. *Nutrients*. 2023;15(4).
11. Wu B, Huang JF, He BJ et al, et al. Promotion of bone formation by red yeast rice in experimental animals: A systematic review and meta-analysis. *Biomed Res Int*. 2020,Aug 8;2020:7231827. doi:10.1155/2020/7231827
12. Yang KL, Mullins BJ, Lejeune A, et al. Short chain fatty acids mitigate osteoclast-mediated arthritic bone remodelling. *Arthritis Rheumat*. 2023.
13. Zhang YW, Cao MM, Li YJ, et al. Fecal microbiota transplantation ameliorates bone loss in mice with ovariectomy-induced osteoporosis via modulating gut microbiota and metabolic function. *J Orthop Translat*. 2022,Sep 26;37():46–60. doi:10.1016/j.jot.2022.08.003
14. Li B, Liu M, Wang Y, et al. Puerarin improves the bone micro-environment to inhibit OVX-induced osteoporosis via modulating SCFAs released by the gut microbiota and repairing intestinal mucosal integrity. *Biomed Pharmacothe*. 2020;132:110923. doi:10.1016/j.biopha.2020.110923
15. Ticinesi A, Siniscalchi C, Meschi, T et al. Gut microbiome and bone health: update on mechanisms, clinical correlations, and possible treatment strategies. *Osteoporos Int*. 2024,Dec 7;():. doi:10.1007/s00198-024-07320-0
16. Zhang H, Qin S, Zhu Y, et al. Dietary resistant starch from potato regulates bone mass by modulating gut microbiota and concomitant short-chain fatty acids production in meat ducks. *Front Nutri*. 2022;9:860086. doi:10.3389/fnut.2022.860086
17. Lucas S, Omata Y, Hofmann J, et al. Short-chain fatty acids regulate systemic bone mass and protect from pathological bone loss. *Nat Commun*. 2018;9(1):55. doi:10.1038/s41467-017-02490-4
18. Carbone AM, Borges JI, Suster MS, et al. Regulator of G-protein signaling-4 attenuates cardiac adverse remodeling and neuronal norepinephrine release-promoting free fatty acid receptor FFAR3 signaling. *Int J Mol Sci*. 2022;23(10):5803. doi:10.3390/ijms23105803
19. Sun M, Wu W, Liu Z, Cong Y. Microbiota metabolite short chain fatty acids, GPCR, and inflammatory bowel diseases. *J Gastroenterol*. 2017;52 (1):1–8. doi:10.1007/s00535-016-1242-9
20. Wu YL, Zhang CH, Teng Y, et al. Propionate and butyrate attenuate macrophage pyroptosis and osteoclastogenesis induced by CoCrMo alloy particles. *Military Medical Research*. 2022;9(1):46. doi:10.1186/s40779-022-00404-0
21. Kobayashi M, Mikami D, Kimura H, et al. Short-chain fatty acids, GPR41 and GPR43 ligands, inhibit TNF-α-induced MCP-1 expression by modulating p38 and JNK signaling pathways in human renal cortical epithelial cells. *Biochem Biophys Res Commun*. 2017;486(2):499–505. doi:10.1016/j.bbrc.2017.03.071
22. Lee K, Seo I, Choi MH, Jeong D. Roles of mitogen-activated protein kinases in osteoclast biology. *Int J Mol Sci*. 2018;19(10):3004. doi:10.3390/ ijms19103004
23. Zaiss MM, Jones RM, Schett G, Pacifici R. The gut-bone axis: how bacterial metabolites bridge the distance. *J Clin Invest*. 2019;129 (8):3018–3028. doi:10.1172/JCI128521
24. Charles JF, Ermann J, Aliprantis AO. The intestinal microbiome and skeletal fitness: connecting bugs and bones. Clin Immunol. 2015;159 (2):163–169.
25. Vich Vila A, Imhann F, Collij V, et al. Weersma, gut microbiota composition and functional changes in inflammatory bowel disease and irritable bowel syndrome. *Sci Trans Med*. 2018;10(472). doi:10.1126/scitranslmed.aap8914
26. Huang F, Pan H, Tan Z et al. Prevotella histicola Prevented Particle-Induced Osteolysis via Gut Microbiota-Dependent Modulation of Inflammation in Ti-Treated Mice. *Probiotics Antimicrob Proteins*. 2024,Apr;16(2):383–393. doi:10.1007/s12602-023-10057-7
27. Wallimann A, Magrath W, Thompson K, et al. Gut microbial-derived short-chain fatty acids and bone: a potential role in fracture healing. *Eur Cells Mater*. 2021;41:454–470. doi:10.22203/eCM.v041a29
28. Xu J, Wu HF, Ang ES, et al. NF-kappaB modulators in osteolytic bone diseases. *Cytokine Growth Factor Rev*. 2009;20(1):7–17. doi:10.1016/j. cytogfr.2008.11.007
29. Ikeda F, Nishimura R, Matsubara T, et al. Critical roles of c-Jun signaling in regulation of NFAT family and RANKL-regulated osteoclast differentiation. *J Clin Invest*. 2004;114(4):475–484. doi:10.1172/JCI200419657
30. Takayanagi H. The role of NFAT in osteoclast formation. *Ann NY Acad Sci*. 2007;1116:227–237. doi:10.1196/annals.1402.071
31. Lee YD, Kim B, Jung S, et al. The dynactin subunit DCTN1 controls osteoclastogenesis via the Cdc42/PAK2 pathway. *Exp Mol Med*. 2020,Mar;52 (3):514–528. doi:10.1038/s12276-020-0406-0
32. Kang MR, Jo SA, Yoon YD, et al. Agelasine D suppresses RANKL-induced osteoclastogenesis via down-regulation of c-Fos, NFATc1 and NF-κB. *Mar Drugs*. 2014;12(11):5643–5656. doi:10.3390/md12115643
33. Matsumoto M, Kogawa M, Wada S, et al. Essential role of p38 mitogen-activated protein kinase in cathepsin K gene expression during osteoclastogenesis through association of NFATc1 and PU.1. *J Biolog Chem*. 2004;279(44):45969–45979. doi:10.1074/jbc.M408795200

34. Villa I, Senesi P, Montesano A, et al. Betaine promotes cell differentiation of human osteoblasts in primary culture. *J Transl Med*. 2017;15(1):132. doi:10.1186/s12967-017-1233-5
35. Xu Y, Chen S, Yu T, Qiao J, Sun G. High-throughput metabolomics investigates anti-osteoporosis activity of oleanolic acid via regulating metabolic networks using ultra-performance liquid chromatography coupled with mass spectrometry. *Phytomedicine*. 2018;51:68–76. doi:10.1016/j.phymed.2018.09.235
36. Wang Y, Che L, Chen X, et al. Repurpose dasatinib and quercetin: targeting senescent cells ameliorates postmenopausal osteoporosis and rejuvenates bone regeneration. *Bioactive Mater*. 2023;25:13–28. doi:10.1016/j.bioactmat.2023.01.009
37. Lee CG, Kim J, Yun SH, et al. Anti-osteoporotic effect of morroniside on osteoblast and osteoclast differentiation in vitro and ovariectomized mice in vivo. *Int J Mol Sci*. 2021;22(19).
38. Liang QL, Xu HG, Yu L, et al. Binding-induced fibrillogenesis peptide inhibits RANKL-mediated osteoclast activation against osteoporosis. *Biomaterials*. 2023;302:122331. doi:10.1016/j.biomaterials.2023.122331

Drug Design, Development and Therapy

Dovepress
Taylor & Francis Group

Publish your work in this journal

Drug Design, Development and Therapy is an international, peer-reviewed open-access journal that spans the spectrum of drug design and development through to clinical applications. Clinical outcomes, patient safety, and programs for the development and effective, safe, and sustained use of medicines are a feature of the journal, which has also been accepted for indexing on PubMed Central. The manuscript management system is completely online and includes a very quick and fair peer-review system, which is all easy to use. Visit http://www.dovepress.com/testimonials.php to read real quotes from published authors.

Submit your manuscript here: https://www.dovepress.com/drug-design-development-and-therapy-journal